

Singular Perturbation Theory for DC–DC Converters and Application to PFC Converters

Jonathan W. Kimball, *Senior Member, IEEE*, and Philip T. Krein, *Fellow, IEEE*

Abstract—Many control schemes for dc–dc converters begin with the assertion that inductor currents are “fast” states and capacitor voltages are “slow” states. This assertion must be true for power factor correction (PFC) converters to allow independent control of current and voltage, and is important for many other applications. In the present study, singular perturbation theory is applied to two-state switching-power converters to provide rigorous justification of the timescale separation. Krylov–Bogoliubov–Mitropolsky averaging is used to include switching ripple effects. A relationship between inductance, capacitance, load resistance, and loss resistances derives from an analysis of the off-manifold dynamics of an approximate model. Similar results hold for boost, buck, and buck–boost converters. Experimental boost converters validate the results. Discrete-time analysis is also shown. Simulated PFC converters demonstrate a simple, sensorless control technique that requires timescale separation.

Index Terms—Averaging, integral manifold, power factor correction (PFC), singular perturbation, stability.

I. INTRODUCTION

CONVENTIONAL wisdom in power electronics is that in dc–dc converters and many other applications, inductor currents are “fast” state variables, while capacitor voltages are “slow” state variables. Often, this is used as justification for a particular design methodology or control scheme. Rarely, if ever, is the assertion verified. As power conversion densities increase, switching frequencies increase, control bandwidths increase, and components are miniaturized, a designer should wonder whether the conventional wisdom is still valid.

Frequently, controllers for dc–dc converters use two loops: an inner current loop and an outer voltage loop. The current loop can take many forms. In an analog controller, the most common approach is peak current mode, where the inductor current is compared to a reference to generate pulsewidth modulation (PWM) gate commands. Average current mode, hysteresis current control, sensorless current mode, and delta modulation are all well-known current control schemes. In the digital realm, several methods have been proposed [1]–[10], most of which fundamentally assume that capacitor voltage remains fixed for

the duration of a switching cycle. The current reference in a two-loop controller is determined through feedback on output voltage. If there is a separation in timescales between the current dynamics and voltage dynamics, the two loops can be designed independently.

While timescale separation is important for many dc–dc converters, power factor correction (PFC) converters *require* separation for proper operation. The objective of a PFC converter is to force an inductor current to follow the input voltage waveform (normally a rectified sinusoid), while the output capacitor voltage is as close to dc as possible [11]. The typical solution is to use a large output capacitor to smooth out the power fluctuations from the input. The conclusion of the analysis to follow, which extends the preliminary work of [12] and [13], is that a sufficiently large capacitor is indeed an alternative that creates timescale separation.

Singular perturbation theory [14] is a tool for formally partitioning a dynamic system into slow and fast variables. The two timescales differ in scale by a small factor of ε . The fast variables, denoted here as \mathbf{z} , are related to the slow variables, denoted as \mathbf{x} , by an integral manifold (an algebraic relation) plus a small dynamic error $\boldsymbol{\eta}$ that is $O(\varepsilon)$. Section II summarizes singular perturbation theory in the present context.

Section III starts with a switched-linear model of a boost converter, which is then normalized to show the variable relationships and identify suitable timescale separation. Krylov–Bogoliubov–Mitropolsky (KBM) averaging yields a nonlinear time-invariant model that includes a ripple correction term [15]. This model fits the standard form for singular perturbation analysis. An approximate model is shown to be suitable only if the converter parameters meet a constraint derived from the off-manifold dynamics. An experimental converter demonstrates the effect of the additional constraint on dynamics. Similar results are shown in Section IV for buck and buck–boost converters. Section V derives corresponding conditions for timescale separation in a discrete-time system. Section VI shows simulations of two PFC converters to demonstrate the effect of timescale separation on dynamic performance. Section VII summarizes the key results.

II. SINGULAR PERTURBATION THEORY

A singularly perturbed system is a nonlinear time-invariant system whose states can be partitioned into slow variables \mathbf{x} and fast variables \mathbf{z} . The separation in timescales is determined by a small scalar ε . The system must be in standard form, where all variables and coefficients are normalized, to apply this method.

Manuscript received January 17, 2008; revised May 8, 2008. This work was supported in part by the National Science Foundation (NSF) under NSF Award ECS 06-21643. Recommended for publication by Associate Editor S. D. Pekarek.

J. W. Kimball is with Missouri University of Science and Technology, Rolla, MO 65409 USA (e-mail: kimballjw@mst.edu).

P. T. Krein is with the Department of Electrical and Computer Engineering, University of Illinois at Urbana-Champaign, Urbana, IL 61801 USA.

Color versions of one or more of the figures in this paper are available online at <http://ieeexplore.ieee.org>.

Digital Object Identifier 10.1109/TPEL.2008.2004272

The standard form for an autonomous system is

$$\begin{aligned}\dot{\mathbf{x}} &= \mathbf{f}(\mathbf{x}, \mathbf{z}, \varepsilon) \\ \varepsilon \dot{\mathbf{z}} &= \mathbf{g}(\mathbf{x}, \mathbf{z}, \varepsilon).\end{aligned}\quad (1)$$

The functions \mathbf{f} and \mathbf{g} may be nonlinear. Switching-power converters also include a control input \mathbf{u} and disturbance input \mathbf{w} . The results to follow hold so long as \mathbf{u} and \mathbf{w} are exogenous (they do not depend on \mathbf{x} or \mathbf{z}). The extended standard form is

$$\begin{aligned}\dot{\mathbf{x}} &= \mathbf{f}(\mathbf{x}, \mathbf{z}, \mathbf{u}, \mathbf{w}, \varepsilon) \\ \varepsilon \dot{\mathbf{z}} &= \mathbf{g}(\mathbf{x}, \mathbf{z}, \mathbf{u}, \mathbf{w}, \varepsilon).\end{aligned}\quad (2)$$

For $\varepsilon \ll 1$, the dynamics can be separated into two timescales. On the fast timescale, \mathbf{x} can be treated as constant while the dynamics of \mathbf{z} are analyzed. On the slow timescale, \mathbf{z} can be treated as algebraic, rather than dynamic, while the dynamics of \mathbf{x} are analyzed. In steady state, the fast variable \mathbf{z} must lie on an integral manifold given by

$$\begin{aligned}\lim_{t \rightarrow \infty} \mathbf{z} &= \phi(\mathbf{x}, \mathbf{u}, \mathbf{w}, \varepsilon) \\ &= \varphi_0(\mathbf{x}, \mathbf{u}, \mathbf{w}, \varepsilon) + \varepsilon \varphi_1(\mathbf{x}, \mathbf{u}, \mathbf{w}, \varepsilon) + O(\varepsilon^2).\end{aligned}\quad (3)$$

The algebraic function ϕ is the exact manifold, whereas a Taylor series approximation is listed on the right. The $O(\varepsilon^2)$ terms can often be neglected, retaining φ_1 improves accuracy for moderate values of ε . During a transient, \mathbf{z} may not lie on the manifold; instead

$$\mathbf{z} = \phi(\mathbf{x}, \mathbf{u}, \mathbf{w}, \varepsilon) + \boldsymbol{\eta} \approx \varphi_0(\mathbf{x}, \mathbf{u}, \mathbf{w}, \varepsilon) + \varepsilon \varphi_1(\mathbf{x}, \mathbf{u}, \mathbf{w}, \varepsilon) + \boldsymbol{\eta} \quad (4)$$

i.e., $\boldsymbol{\eta}$ is a new state variable that captures the dynamics of the transition from an arbitrary point in the state space to a point on the manifold, after which (3) applies.

A complete derivation of the approximate model $\mathbf{z} = \varphi_0 + \varepsilon \varphi_1 + \boldsymbol{\eta}$ is given in [14] and is summarized here. The left-hand side of the original $\dot{\mathbf{z}}$ equation evaluated along the manifold is

$$\varepsilon \frac{d\mathbf{z}}{dt} = \varepsilon \frac{d\phi}{dt} = \varepsilon \frac{\partial \phi}{\partial \mathbf{x}} \frac{d\mathbf{x}}{dt}. \quad (5)$$

Combining (2) and (5),

$$\varepsilon \frac{\partial \phi}{\partial \mathbf{x}} \mathbf{f}(\mathbf{x}, \phi, \mathbf{u}, \mathbf{w}, \varepsilon) = \mathbf{g}(\mathbf{x}, \phi, \mathbf{u}, \mathbf{w}, \varepsilon). \quad (6)$$

Next, substitute the Taylor series (3) and equate powers of ε to find φ_0 and φ_1

$$\begin{aligned}\varepsilon^0 : \quad 0 &= \mathbf{g}(\mathbf{x}, \varphi_0, \mathbf{u}, \mathbf{w}, 0) \\ \varepsilon^1 : \quad \frac{\partial \varphi_0}{\partial \mathbf{x}} \mathbf{f}(\mathbf{x}, \varphi_0, \mathbf{u}, \mathbf{w}, \varepsilon) &= \frac{\partial \mathbf{g}}{\partial \mathbf{z}} \varphi_1.\end{aligned}\quad (7)$$

The dynamical equation for $\boldsymbol{\eta}$ can be found by subtracting the contributions of the φ_0 and φ_1 from the \mathbf{z} dynamical equation. In terms of (4), the equation for $\dot{\mathbf{z}}$ can be written as

$$\varepsilon \frac{d}{dt} (\varphi_0 + \varepsilon \varphi_1 + \boldsymbol{\eta}) = \mathbf{g}(\mathbf{x}, \varphi_0 + \varepsilon \varphi_1 + \boldsymbol{\eta}, \mathbf{u}, \mathbf{w}, \varepsilon). \quad (8)$$

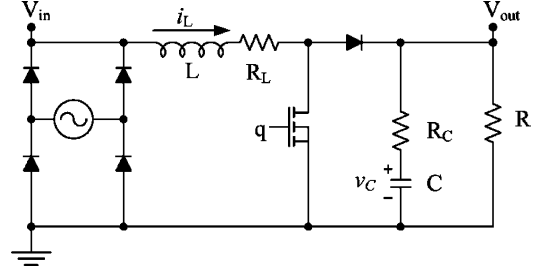


Fig. 1. Boost PFC converter.

This equation can be reduced since φ_0 and φ_1 are known from (7), and their time derivatives are given by the chain rule

$$\frac{d}{dt} (\varphi_0 + \varepsilon \varphi_1) = \left(\frac{\partial \varphi_0}{\partial \mathbf{x}} + \varepsilon \frac{\partial \varphi_1}{\partial \mathbf{x}} \right) \mathbf{f}(\mathbf{x}, \varphi_0 + \varepsilon \varphi_1 + \boldsymbol{\eta}, \mathbf{u}, \mathbf{w}, \varepsilon). \quad (9)$$

Depending on form and system details, it may or may not be feasible to find a useful form of $\boldsymbol{\eta}$ from (9). A critical requirement is that (8) is stable, i.e., the off-manifold dynamics $\boldsymbol{\eta}$ must decay so that the state vector will converge to the manifold.

The following sections will find timescale separation criteria for two-state dc-dc converters: boost, buck, and buck-boost. State-space averaged models of these power converters fit the generic form

$$\dot{\mathbf{x}} = (\mathbf{A}_1 + \mathbf{A}_2 D) \mathbf{x} + (\mathbf{B}_1 + \mathbf{B}_2 D) \mathbf{w} \quad (10)$$

where \mathbf{x} is the state vector, D is the duty cycle, \mathbf{w} is a disturbance input (such as input voltage or load), and \mathbf{A}_1 , \mathbf{A}_2 , \mathbf{B}_1 , and \mathbf{B}_2 determine the overall operation of the converter.

For the two state converters discussed in this paper, many of the elements of the matrices in (10) are zero. Therefore, the analysis is more straightforward for particular cases than for the generic case (10). Other averaging techniques also yield nonlinear forms that must be analyzed on a case-by-case basis.

In buck, boost, and buck-boost converters, the partitioned subsystems for the two different timescales are scalar. The control input is related to the switching function. The disturbance input is the converter input voltage. As will be shown, there is a crucial relationship among the converter parameters that determines whether the off-manifold dynamics are stable. If they are not, then one cannot, in general, treat capacitor voltages and inductor currents as operating on different timescales. Initially, the load will be treated as a constant resistance. Later, a Norton equivalent load will be considered to generalize the analysis to constant-power loads.

III. BOOST CONVERTER ANALYSIS

A. Switched Linear Model

The open-loop PFC boost converter shown in Fig. 1 can be modeled as a switched linear system. A closed-loop version would be nonlinear and time-varying. The PFC application

implies large variation in input voltage and inductor current; otherwise, the dynamics are identical to any other boost converter. The switched linear model is

$$\begin{aligned}\frac{dv_C}{dt} &= -\frac{1}{C(R+R_C)}v_C + h_2 \frac{R}{C(R+R_C)}i_L \\ \frac{di_L}{dt} &= -h_2 \frac{R}{L(R+R_C)}v_C - \frac{R_L + h_2(R\parallel R_C)}{L}i_L + \frac{v_{in}}{L}.\end{aligned}\quad (11)$$

Here, h_2 is the switching function of the diode. All variables and coefficients must be normalized to put the system into standard form. The nominal output voltage is V_0 , the nominal output current is $I_0 = V_0/R$, and the switching period is T . With these definitions, the other variables can be normalized on the basis

$$\begin{aligned}\hat{v}_C &= \frac{v_C}{V_0} \\ \hat{i}_L &= \frac{i_L}{I_0} = \frac{i_L R}{V_0} \\ w &= \frac{v_{in}}{V_0} \\ u &= 1 - d = \langle h_2 \rangle \\ \hat{t} &= \frac{t}{C(R+R_C)} \\ p &= \frac{T}{C(R+R_C)} \\ \delta_0 &= \frac{R_L R + R_C}{R} \\ \varepsilon &= \frac{L}{R^2 C}.\end{aligned}\quad (12)$$

The first two variables are the normalized states. Normalized input voltage w is a disturbance input. The moving average of h_2 , shown as u , is used as the input in the following analysis; often, the actual input is d , the duty cycle of the controlled switch. Time must be normalized (\hat{t}) so that the timescale of the slow variable \hat{v}_C is $O(1)$. Then, the switching period T must be transformed into p on the \hat{t} timescale. The last two variables accumulate the various parameters of the physical system. The normalized switched dynamical system is

$$\frac{d}{d\hat{t}} \begin{bmatrix} \hat{v}_C \\ \hat{i}_L \end{bmatrix} = \begin{bmatrix} -1 & h_2 \\ -\frac{h_2}{\varepsilon} & -\frac{\delta_0 + h_2 \frac{R_C}{R}}{\varepsilon} \end{bmatrix} \begin{bmatrix} \hat{v}_C \\ \hat{i}_L \end{bmatrix} + \begin{bmatrix} 0 \\ \frac{R_C + R}{\varepsilon R} \end{bmatrix} w.\quad (14)$$

B. Averaged System

Averaging can be applied to (14) to enable further analysis. Although singular perturbation theory may be applied to time-varying systems, the switching power converter results are more readily applied if the system is first converted to an equivalent time-invariant system. Since h_2 is a switching function, the model (14) is linear in the states but time-varying. State-space

averaging [16]–[18], which removes all knowledge of switching frequency, is typically used to form a nonlinear time-invariant converter model. Other averaging methods retain switching information in time-invariant models. In particular, KBM averaging [15], [19], [20] is an algorithm that partitions a periodically varying system

$$\dot{\xi} = \alpha \mathbf{F}(t, \xi) \quad (15)$$

into a time-varying algebraic relationship

$$\xi(t) = \mathbf{y}(t) + \alpha \Psi_1(t, \mathbf{y}) + \alpha^2 \Psi_2(t, \mathbf{y}) + \dots \quad (16)$$

and a time-invariant dynamical system

$$\dot{\mathbf{y}} = \alpha \mathbf{G}_1(\mathbf{y}) + \alpha^2 \mathbf{G}_2(\mathbf{y}) + \alpha^3 \mathbf{G}_3(\mathbf{y}) + \dots \quad (17)$$

The new state vector \mathbf{y} corresponds to a moving average of the original states ξ , while the algebraic series in Ψ models the ripple. The series in \mathbf{G} is time-invariant and admits further analysis. KBM averaging differs from generalized state-space averaging [21] primarily in the choice of basis functions. Whereas generalized state-space averaging uses a Fourier approach (sinusoidal bases), the KBM approach as in [15] uses piecewise polynomials. Since most useful signals in a hard-switching power converter are piecewise exponential, one would expect a summation of piecewise polynomial functions to fit the real signals with fewer terms than a summation of sinusoids. Terms past Ψ_3 are usually negligible in real dc–dc converters.

The switched linear system (14) fits the basic form of (15), so KBM averaging applies. Mathematica¹ was used to find \mathbf{G} and Ψ terms (see the Appendix for code listing, adapted and extended from [19]). For a boost converter, \mathbf{G}_1 is the conventional state-space average and \mathbf{G}_2 is identically zero. The term \mathbf{G}_3 is $O((p/\varepsilon)^2)$ and captures effects of piecewise linear ripple on the states at the switching frequency. For a reasonable switching frequency, higher order terms diminish rapidly. The averaged form through \mathbf{G}_3 , found with Mathematica, is

$$\begin{aligned}\frac{dy_1}{d\hat{t}} &= uy_2 - y_1 - \frac{1}{12} \left(\frac{u(1-u)p}{\varepsilon} \right)^2 \\ &\quad \times \left(y_1(\delta_0 - \varepsilon) + \frac{R_C}{R} \frac{R+R_C}{R} w \right) \\ \varepsilon \frac{dy_2}{d\hat{t}} &= \frac{R+R_C}{R} w - uy_1 - \left(\delta_0 + \frac{R_C}{R} u \right) y_2 \\ &\quad + \frac{1}{12} \left(\frac{u(1-u)p}{\varepsilon} \right)^2 \left(y_1 \frac{R_C}{R} (\delta_0 - \varepsilon) + y_2 \varepsilon (\delta_0 - \varepsilon) \right. \\ &\quad \left. + \frac{R_C + R}{R} w \left(\frac{R_C^2}{R^2} - \varepsilon \right) \right).\end{aligned}\quad (18)$$

A three-step analysis of (18) will establish timescale separation criteria. First, the state-space-averaged system (\mathbf{G}_1 , which does not include the terms proportional to $(p/\varepsilon)^2$) will be analyzed symbolically to find a simple relationship that determines whether or not timescales separate in a given converter. Then,

¹Mathematica is a registered trademark of Wolfram Research, Inc.

results from an experimental converter will verify the conclusions. Finally, the actual parameters of the experimental converter will be substituted into (18) numerically to show that \mathbf{G}_3 has a minor effect on timescale phenomena since it is small for a converter in continuous conduction mode.

C. Singular Perturbation Analysis

To put the averaged model (18) into standard form (2), we identify $x = y_1$ and $z = y_2$, and neglect all terms except \mathbf{G}_1 . Thus

$$\begin{aligned} \frac{dx}{dt} &= f(x, z, u), w, \varepsilon = uz - x \\ \varepsilon \frac{dz}{dt} &= g(x, z, u, w, \varepsilon) = \frac{R + R_C}{R} w - ux - \left(\delta_0 + \frac{R_C}{R} u \right) z. \end{aligned} \quad (19)$$

All coefficients on the right-hand side must be normalized for singular perturbation analysis. Typically, the equivalent series resistance (ESR) term $R_C \ll R$, so the coefficient of w in the second equation is a few percent larger than unity. The coefficient of z , though, is small for a highly efficient converter. This coefficient is defined to be

$$\delta(u) = \delta_0 + \frac{R_C}{R} u. \quad (20)$$

The effect of this small but nonzero coefficient $\delta(u)$ can be determined from an analysis of the approximate model (4). The main contribution to the integral manifold is φ_0 , which is found by solving the first equation in (7) for φ_0 to find

$$\varphi_0 = \frac{w(1 + (R_C/R)) - ux}{\delta(u)}. \quad (21)$$

Next, the first-order correction φ_1 can be found from the second equation in (7) as

$$\begin{aligned} \varphi_1 &= \left(\frac{\partial g}{\partial z} \right)^{-1} \left(\frac{\partial \varphi_0}{\partial x} \right) f(x, \varphi_0, u, w, \varepsilon) \\ \varphi_1 &= \frac{u^2 w ((R + R_C)/R) - u^3 x - ux \delta(u)}{\delta^3(u)}. \end{aligned} \quad (22)$$

The off-manifold dynamics can be found from (8), (21), and (22), which simplify substantially to

$$\varepsilon \frac{d\eta}{dt} = \left(\frac{\varepsilon u^2}{\delta(u)} - \delta(u) \right) \eta. \quad (23)$$

To complete the new system, an approximate dynamical equation for x can be found as

$$\begin{aligned} \frac{dx}{dt} &= u(\varphi_0 + \varepsilon \varphi_1) - x = (\alpha_{\text{boost}} x + \beta_{\text{boost}} w) \gamma_{\text{boost}} \\ \alpha_{\text{boost}} &= - (u^2 + \delta(u)) \\ \beta_{\text{boost}} &= \frac{R + R_C}{R} u \\ \gamma_{\text{boost}} &= \frac{\delta^2(u) + u^2 \varepsilon}{\delta^3(u)}. \end{aligned} \quad (24)$$

TABLE I
BASIC CONVERTER PARAMETERS

L	657 μH	C	77 μF
R_L	584 $\text{m}\Omega$	R_C	381 $\text{m}\Omega$
MOSFET	IRF3710	Diode	MBR1545CT
ε	8.5×10^{-4}	δ_0	5.9×10^{-3}
Frequency	25 kHz	p	5.2×10^{-3}
R	100 Ω		

Although the input u enters in a complicated fashion, the dynamics of x are linear in both x and w for a given duty cycle. So, a boost converter that exhibits timescale separation will have first-order capacitor voltage dynamics in response to a step change in duty cycle after a brief current transient (the decay of off-manifold dynamics).

The basic concept of a singularly perturbed system is that the fast dynamics decay rapidly. Then, z will normally be on or near the integral manifold ϕ , and the relationship between x and z will be dominantly algebraic, rather than dynamic. This requires η to have a stable equilibrium near the origin. A stable, nonzero equilibrium is acceptable, but unstable dynamics are not. Stability of (23) requires the coefficient of η to be negative. Algebraic manipulation gives a stability requirement

$$\varepsilon u^2 < \delta^2(u). \quad (25)$$

If the converter parameters satisfy (25) at a given operating point, then there exists a separation between the dynamics of x and z , or equivalently, between v_C and i_L .

The requirement (25) is a function of the exogenous input u , while a designer would prefer a universally applicable requirement. To generalize, a stricter requirement can be found that does not include u , given that $u \in [0, 1]$

$$\varepsilon < \delta_0^2. \quad (26)$$

Both ε and δ_0 include the load resistance R in their definitions. An even stricter requirement can be found that does not include R

$$\sqrt{\frac{L}{C}} < R_L. \quad (27)$$

Equation (27) implies that the equivalent series LRC circuit formed by the inductor, its parasitic resistance, and the output capacitor must be overdamped (quality factor $Q < 1$). The key contribution of the present study is a rigorous derivation of these timescale separation requirements from basic circuit theory, nonlinear system theory, and singular perturbation theory.

D. Experimental Verification

A boost converter was constructed to demonstrate the relevance of (27). Parameters are listed in Table I, with MOSFET resistance lumped into R_L . The design specification is for 12–36 V conversion at 13 W. As constructed, this converter does not meet the requirement for timescale separation. The

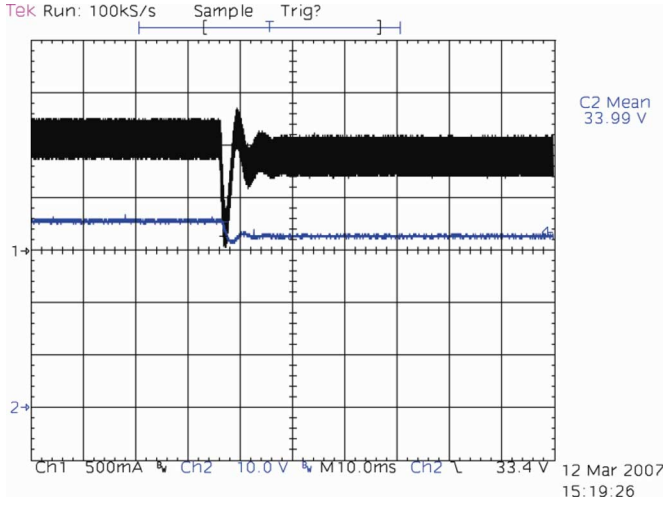


Fig. 2. Experimental duty cycle step (67%–64%) with original converter. Note second-order behavior. (Top waveform) Channel 1, inductor current 500 mA/division. (Bottom waveform) Channel 2, output voltage 10 V/division. Horizontal: 10 ms/division.

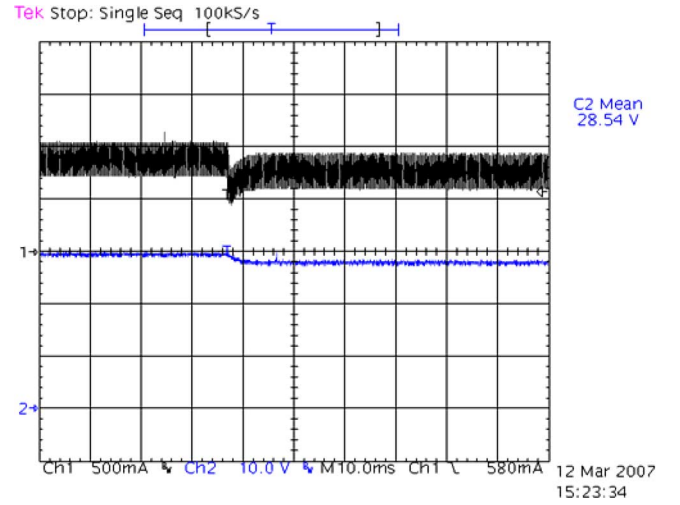


Fig. 3. Experimental duty cycle step (67%–64%) with added resistance in inductor (2 Ω). (Top waveform) Channel 1, inductor current 500 mA/division. (Bottom waveform) Channel 2, output voltage 10 V/division. Horizontal: 10 ms/division.

characteristic impedance is $\sqrt{L/C} = 2.92 \Omega$, which exceeds R_L by about a factor of 5. For the experimental converter, small duty cycle steps were applied to ensure that the inductor current remains continuous. If the current becomes discontinuous, then the averaged model (18) is no longer accurate.

With the converter that fails the separation criteria, a duty cycle step was applied, from 67% to 64%. Inductor current and output voltage are shown in Fig. 2. Classic second-order behavior is seen, which indicates that the state dynamics are closely coupled. Efficiency is approximately 95%. Two different approaches were then used to achieve the timescale separation requirement.

Fig. 3 shows the effect of additional resistance (2 Ω) added in series with the inductor. This increased δ_0 to 0.026 to achieve timescale separation at the price of additional losses. Current and voltage waveforms for the same duty cycle step as before (67%–64%) are shown in Fig. 3. The traces show a fast first-order transient, which indicates decoupling of the two states. Even more resistance would be needed for timescale separation to be effective across a wide range of u . Efficiency was about 81%.

The additional losses are undesirable for a highly efficient power converter, so another approach was examined: additional capacitance. Fig. 4 shows current and voltage trajectories for a smaller step, 67%–66%, where the converter has an additional 2200 μF to reduce ε to 3.16×10^{-5} and decrease p to 1.92×10^{-4} . The efficiency was still high, about 95%. The dynamic behavior in Fig. 4 shows decoupling of the states, but the larger capacitance causes dynamic performance to suffer. The current response to this smaller input transient is larger and decays more slowly than the preceding cases. Fig. 4 most clearly shows the terms that contribute to the approximate model of z . The rapid drop in current is governed by off-manifold dynamics as η decays to zero, while the recovery toward the initial current is

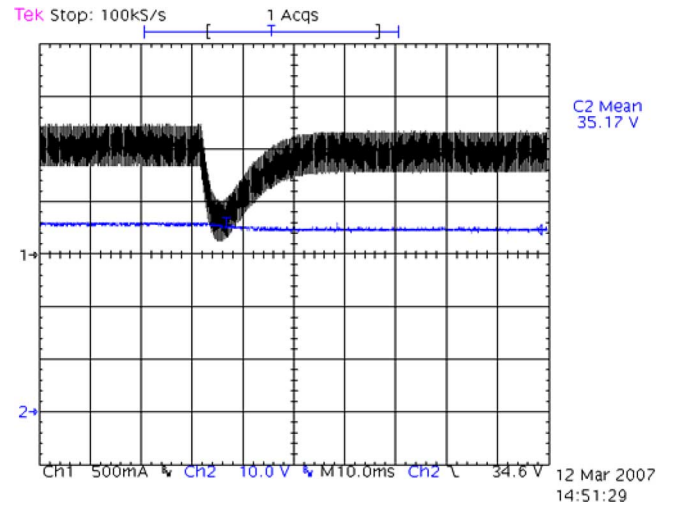


Fig. 4. Experimental duty cycle step (67%–66%) with added output capacitance (2200 μF). (Top waveform) Channel 1, inductor current 500 mA/division. (Bottom waveform) Channel 2, output voltage 10 V/division. Horizontal: 10 ms/division.

governed by decoupled behavior along the integral manifold as the voltage changes.

For the experimental converter, the KBM average can be evaluated numerically, i.e., an approximate model can be derived as in (21)–(24), but with the extra term listed in (18) that was neglected before. The leading coefficient of the \mathbf{G}_3 terms is

$$\frac{1}{12} \left(\frac{u(1-u)p}{\varepsilon} \right)^2 = 0.151. \quad (28)$$

Continuous conduction mode generally corresponds to a leading coefficient less than unity. More formally, the critical

inductance can be substituted to simplify this coefficient

$$\frac{u(1-u)p}{\varepsilon} = \frac{2}{u} \frac{R}{R+R_C} \quad (29)$$

$$\frac{1}{12} \left(\frac{u(1-u)p}{\varepsilon} \right)^2 \approx \frac{1}{3u^2}. \quad (30)$$

So, the leading coefficient will be less than unity for duty cycles less than about 42% in critical conduction mode, and for greater duty cycles as inductance or load is increased. The most important element of the theoretical development is the η dynamic equation. For the three cases, the dynamic equations for η that include \mathbf{G}_3 terms are

$$\begin{aligned} \varepsilon \frac{d\eta}{dt} \Big|_{\text{base}} &= 6.99\eta - 2.60 \times 10^{-13}y_1 + 2.60 \times 10^{-13}w \\ \varepsilon \frac{d\eta}{dt} \Big|_{\text{add } R} &= -27.9\eta - 2.43 \times 10^{-14}y_1 + 1.95 \times 10^{-13}w \\ \varepsilon \frac{d\eta}{dt} \Big|_{\text{add } C} &= -210\eta - 1.21 \times 10^{-12}y_1 - 3.95 \times 10^{-12}w. \end{aligned} \quad (31)$$

In the base case, the coefficient of η is positive, so the approximate model is unstable and timescale separation does not take place as dynamic behavior does not converge to the manifold. In the other two cases, the coefficients of η are negative as desired. Note the orders of magnitude of the y_1 and w terms: since y_1 and w are both $O(1)$, these small terms will only move the η equilibrium value a minute distance from zero. While z will not lie exactly on the integral manifold, the difference has no discernable impact on operation.

The effect of the first-order correction φ_1 can also be evaluated numerically. For the middle case with extra resistance

$$\begin{aligned} \varphi_0 &= -12.1\hat{v}_C + 36.8w \\ \varepsilon\varphi_1 &= -1.90\hat{v}_C + 4.62w. \end{aligned} \quad (32)$$

For the case with extra capacitance

$$\begin{aligned} \varphi_0 &= -46.4\hat{v}_C + 141w \\ \varepsilon\varphi_1 &= -3.36\hat{v}_C + 9.60w. \end{aligned} \quad (33)$$

So, neglecting the first-order correction would degrade accuracy by about 15% for one case, and 7% for the other.

The analysis and experiments agree and show three possible cases. The base converter has fast, coupled dynamics, and exhibits second-order behavior. One variant has higher losses with fast, decoupled dynamics. Another variant has additional capacitance for high efficiency and slow, decoupled dynamics.

E. Other Load Types

The earlier analysis applies to constant-resistance loads. Two other static load types will be analyzed: constant current and constant power. If the load R is replaced with a Norton equivalent, all three load types can be included, at least in a small-signal sense. See Fig. 5 for the new configuration with I_N and R_N .

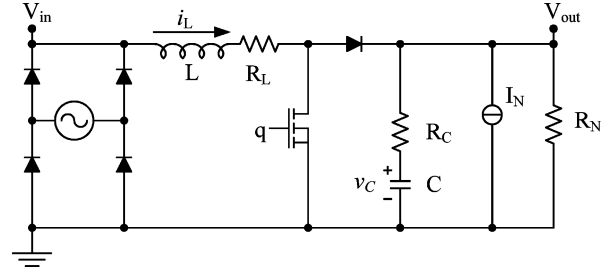


Fig. 5. Boost converter with Norton load.

Generally, I_N is nonnegative, but R_N may be of either sign. If R_N is positive, the current sink changes the equilibrium by some offset, and off-manifold dynamics do not change. For a constant-current load, R_N approaches infinity and ε approaches zero, so the dynamical system is singular. For a constant-power load, I_N is positive and R_N is negative, which requires further analysis. The normalized variables must be changed so that they have the same sign as the physical variables. Typically, $|R_N| > R_C$, and the normalization is

$$\begin{aligned} \hat{v}_C &= \frac{v_C}{V_0} \\ \hat{i}_L &= -\frac{i_L R_N}{V_0} \\ w_1 &= \frac{V_{in}}{V_0} \\ w_2 &= -\frac{I_N R_N}{V_0} \\ u &= \langle h_2 \rangle \\ \hat{t} &= -\frac{t}{C(R_N + R_C)} \\ p &= -\frac{T}{C(R_N + R_C)} \\ \delta_0 &= \frac{R_L R_N + R_C}{R_N R_N} \\ \varepsilon &= \frac{L}{R_N^2 C}. \end{aligned} \quad (34)$$

All variables are positive except δ_0 , which is negative. The switched linear dynamical equations change to

$$\begin{aligned} \frac{d}{dt} \begin{bmatrix} \hat{v}_C \\ \hat{i}_L \end{bmatrix} &= \begin{bmatrix} 1 & h_2 \\ -\frac{h_2}{\varepsilon} & \frac{1}{\varepsilon} \left(\delta_0 + h_2 \frac{R_C}{R_N} \right) \end{bmatrix} \begin{bmatrix} \hat{v}_C \\ \hat{i}_L \end{bmatrix} \\ &+ \begin{bmatrix} w_2 \\ \frac{1}{\varepsilon} \left(\frac{R_C + R_N}{R_N} w_1 - h_2 w_2 \frac{R_C}{R_N} \right) \end{bmatrix}. \end{aligned} \quad (35)$$

As mentioned before, KBM averaging converts this switched linear system into a nonlinear time-invariant system. Singular perturbation analysis yields an approximate model for the

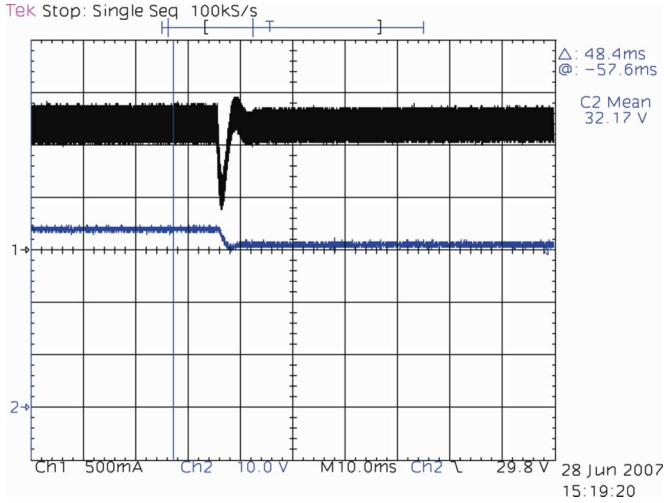


Fig. 6. Experimental duty cycle step (67%–64%) with original converter, now with a constant-power load. (Top waveform) Channel 1, inductor current 500 mA/division. (Bottom waveform) Channel 2, output voltage 10 V/division. Horizontal: 10 ms/division.

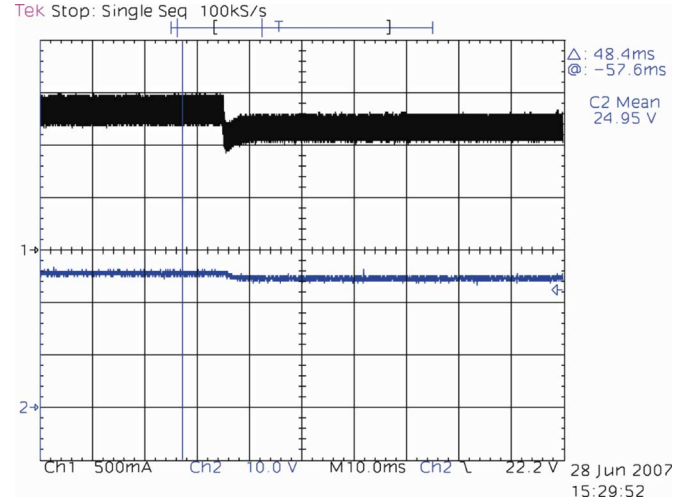


Fig. 7. Experimental duty cycle step (67%–64%) with increased resistance and constant-power load. (Top waveform) Channel 1, inductor current 500 mA/division. (Bottom waveform) Channel 2, output voltage 10 V/division. Horizontal: 10 ms/div.

moving average of \hat{i}_L , plus a differential equation that governs off-manifold dynamics

$$\varepsilon \frac{d\eta}{dt} = \left(\delta(u) - \frac{u^2 \varepsilon}{\delta(u)} \right) \eta. \quad (37)$$

Equation (37) differs only slightly from (22). The small coefficient $\delta(u)$ is the same as in (20), but is now negative. Timescale separation requires stable η dynamics or

$$\delta(u) - \frac{u^2 \varepsilon}{\delta(u)} < 0. \quad (38)$$

With some algebraic manipulation, and with care for sign changes, the stability requirement reduces to

$$u^2 \varepsilon < \delta^2(u). \quad (39)$$

Simplifications can be applied as before and yield the same stability requirement as (27).

F. Experimental Validation With Constant-Power Load

The converters described in Section III-D were tested with a constant-power load. The load consisted of a large bipolar junction transistor (BJT) (D44VH10), 57 Ω of resistive ballast, and a control circuit built around an AD633 analog multiplier. Integral control was used to regulate the load power on a sub-millisecond timescale. The power was set to 13 W to correlate with the previous test points.

Fig. 6 shows the response of the base converter with a constant-power load. As in Fig. 2, the dynamics resemble a second-order system. For Fig. 7, an extra 2 Ω was inserted in series with the inductor. The result is fast, decoupled dynamics. For a constant-power load, reduced converter efficiency causes

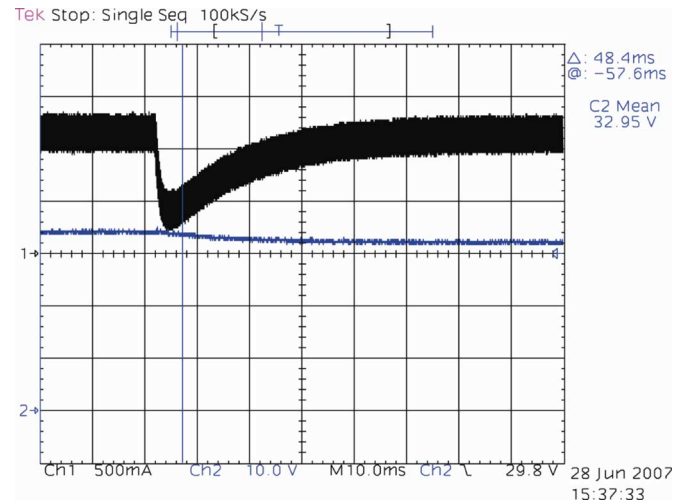


Fig. 8. Experimental duty cycle step (67%–65%) with increased capacitance and constant-power load. (Top waveform) Channel 1, inductor current 500 mA/division. (Bottom waveform) Channel 2, output voltage 10 V/division. Horizontal: 10 ms/division.

changes in duty cycle to dramatically impact the steady-state operating point (both output voltage and inductor current). This can be understood heuristically as follows. A decrease in duty cycle results in a decrease in output voltage, which leads to an increase in output current due to the negative load resistance. The corresponding increase in inductor current results in substantially increased losses, which further reduces the output voltage. In Fig. 8, an extra 1400 μF was added instead of the resistance. High efficiency is retained, but the response time is much longer.

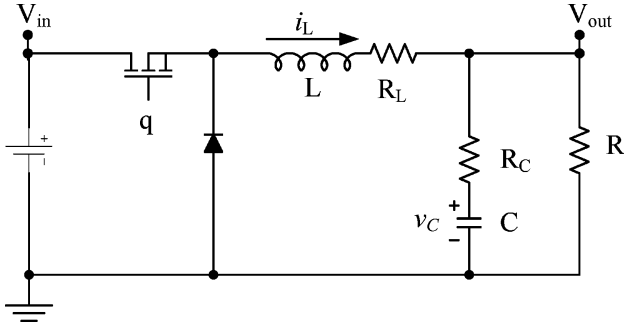


Fig. 9. Buck converter.

To summarize, timescale separation can be achieved for any load that includes a resistive term, whether the resistance is positive or negative. Typically, the inductor will be designed to satisfy ripple current and efficiency requirements. Given the corresponding L and R_L , the designer can choose the capacitor to satisfy (27), and separate voltage and current timescales.

IV. BUCK AND BUCK–BOOST CONVERTERS

Boost, buck, and buck–boost converters are all composed of the same elements—one inductor, one capacitor, one controlled switch, and one diode. For clarity, the same normalized variable definitions of (12) and (13) will be used in the analysis of buck and buck–boost converters.

A buck converter, shown in Fig. 9, has dynamics that are time-invariant in the states. In the KBM average, all terms above \mathbf{G}_1 vanish identically. The normalized, averaged model in singular perturbation standard form is

$$\begin{aligned} \frac{dx}{dt} &= z - x \\ \varepsilon \frac{dz}{dt} &= \frac{R + R_C}{R} (1 - u) w - ux - \left(\delta_0 + \frac{R_C}{R} u \right) z. \end{aligned} \quad (40)$$

The similarities between (19) and (40) are obvious. As might be expected, the approximate model for z is similar to the boost converter case, with x and η dynamics governed by

$$\begin{aligned} \frac{dx}{dt} &= (\alpha_{\text{buck}} x + \beta_{\text{buck}} w) \gamma_{\text{buck}} \\ \alpha_{\text{buck}} &= \delta_0 + \frac{R_C}{R} \\ \beta_{\text{buck}} &= \frac{R + R_C}{R} (1 - u) \\ \gamma_{\text{buck}} &= \frac{\delta_0^2 + u^2 \varepsilon}{\delta_0^3} \end{aligned} \quad (41)$$

$$\varepsilon \frac{d\eta}{dt} = \left(\frac{\varepsilon}{\delta_0} - \delta_0 \right) \eta. \quad (42)$$

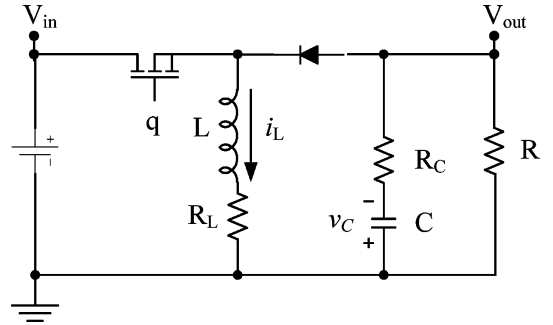


Fig. 10. Buck–boost converter.

The η dynamics are stable for

$$\varepsilon < \delta_0^2. \quad (43)$$

As in the boost converter case, simplifications can be made that result in exactly the same criterion as (27).

The buck–boost converter shown in Fig. 10 has dynamics that are time-varying in the states similarly to a boost converter. Considering only the state-space average (\mathbf{G}_1), the normalized dynamics are

$$\begin{aligned} \frac{dx}{dt} &= uz - x \\ \varepsilon \frac{dz}{dt} &= \frac{R + R_C}{R} (1 - u) w - ux - \left(\delta_0 + \frac{R_C}{R} u \right) z. \end{aligned} \quad (44)$$

Again, similarities to the boost converter model are obvious. The approximate model is

$$\begin{aligned} \frac{dx}{dt} &= (\alpha_{bb} x + \beta_{bb} w) \times \gamma_{bb} \\ \alpha_{bb} &= -(u^2 + \delta(u)) \\ \beta_{bb} &= \frac{R + R_C}{R} u(1 - u) \\ \gamma_{bb} &= \frac{\delta^2(u) + u^2 \varepsilon}{\delta^3(u)} \end{aligned} \quad (45)$$

$$\varepsilon \frac{d\eta}{dt} = \left(\frac{\varepsilon u^2}{\delta(u)} - \delta(u) \right) \eta. \quad (46)$$

The η dynamic equation is identical to that of the boost converter (23), so the stability criterion is identical to (27). The dynamical equation for x differs only in the way u interacts with w . For this converter, \mathbf{G}_2 is zero and \mathbf{G}_3 can be considered numerically. The higher order term has a similar effect on η as in a boost converter.

V. SAMPLED-DATA (DISCRETE-TIME) ANALYSIS

To study singular perturbation in digital controls, a sampled-data model [22], [23] can be analyzed for timescale separation. Generic discrete-time systems have been analyzed with singular perturbation theory [24]–[28]. The boost converter of Fig. 1

demonstrates the basic problem of timescale separation with a digital control. First, the continuous-time model of (14) needs to be converted to discrete time. For notational convenience, rewrite the continuous-time model as

$$\begin{aligned} \frac{d}{dt} \begin{bmatrix} \hat{v}_C \\ \hat{i}_L \end{bmatrix} &= (\mathbf{A}_1 + h_2 \mathbf{A}_2) \begin{bmatrix} \hat{v}_C \\ \hat{i}_L \end{bmatrix} + \mathbf{B}_1 w \\ \mathbf{A}_1 &= \begin{bmatrix} -1 & 0 \\ 0 & -\frac{\delta_0}{\varepsilon} \end{bmatrix} \\ \mathbf{A}_2 &= \begin{bmatrix} 0 & 1 \\ -\frac{1}{\varepsilon} & -\frac{R_C}{\varepsilon R} \end{bmatrix} \\ \mathbf{B} &= \begin{bmatrix} 0 \\ \frac{R_C + R}{\varepsilon R} \end{bmatrix}. \end{aligned} \quad (47)$$

With the input voltage (equivalently, w) and duty cycle (or u) held constant for one cycle p (in normalized time), the discrete-time system can be written as

$$\begin{aligned} \begin{bmatrix} \hat{v}_C \\ \hat{i}_L \end{bmatrix} [k+1] &= \Phi[k] \begin{bmatrix} \hat{v}_C \\ \hat{i}_L \end{bmatrix} [k] + \Gamma[k] w[k] \\ \Phi[k] &= \exp(\mathbf{A}_1(1-u[k]p)) \exp((\mathbf{A}_1 + \mathbf{A}_2)u[k]p) \\ \Gamma[k] &= \frac{\mathbf{A}_1^{-1}}{(1-u[k]p)} (\exp(\mathbf{A}_1(1-u[k]p)) - \mathbf{I})\mathbf{B} \\ &\quad + \frac{(\mathbf{A}_1 + \mathbf{A}_2)^{-1}}{u[k]p} (\exp((\mathbf{A}_1 + \mathbf{A}_2)u[k]p) - \mathbf{I})\mathbf{B}. \end{aligned} \quad (48)$$

The contribution from the input voltage does not enter into the remaining discussion. The state transition matrix Φ can be approximated since

$$\exp(\mathbf{A}t) = \mathbf{I} + \mathbf{A}t + O((\mathbf{A}t)^2). \quad (49)$$

Discarding all terms quadratic in time p

$$\Phi[k] \approx (\mathbf{I} + \mathbf{A}_1(1-u[k]p))(\mathbf{I} + (\mathbf{A}_1 + \mathbf{A}_2)u[k]p). \quad (50)$$

Expand (50), substitute the actual values of \mathbf{A}_1 and \mathbf{A}_2 , and again discard all terms quadratic in p to yield

$$\Phi[k] \approx \begin{bmatrix} 1-p & u[k]p \\ -\frac{u[k]p}{\varepsilon} & 1 - \frac{u[k]p}{\varepsilon} \frac{R_C}{R} - \frac{p\delta_0}{\varepsilon} \end{bmatrix}. \quad (51)$$

TABLE II
EXPERIMENTAL BOOST CONVERTER IN SAMPLED-DATA FRAMEWORK

Experimental Case	Satisfies (55)?	Satisfies (54)?	Eigenvalues
Base	0.584 < 5.8421 NO	$3.93 \times 10^{-5} < 3.72 \times 10^{-4}$ NO	0.9761 ± j0.0554
Add 2 Ω to R_L	2.584 < 5.8421 NO	$6.94 \times 10^{-4} > 3.72 \times 10^{-4}$ YES	0.9678, 0.8684
Add 2.2 mF to C	0.584 < 1.0743 NO	$5.03 \times 10^{-5} > 1.26 \times 10^{-5}$ YES	0.9969, 0.9602

The approximated state transition matrix does not satisfy the criteria in [24]. However, it is possible to check whether the eigenvalues are real and distinct, rather than complex conjugate. If so, then some degree of timescale separation and decoupling would be expected.

The eigenvalues of Φ (as approximated in (51), with the time index k implicit) are

$$\begin{aligned} 1 + \frac{p}{2\varepsilon} \left(u \frac{R_C}{R} + \delta_0 \right) + \frac{p}{2} \pm \sqrt{\text{DISCRIMINANT}} \\ \text{DISCRIMINANT} = \frac{p^2}{4\varepsilon^2} \left(\left(\frac{R_C}{R} u + \delta_0 - \varepsilon \right)^2 - 4u^2\varepsilon \right). \end{aligned} \quad (52)$$

The eigenvalues will be real and distinct if

$$\text{DISCRIMINANT} > 0. \quad (53)$$

With (52) substituted into (53)

$$\left(\frac{R_C}{R} u + \delta_0 - \varepsilon \right)^2 > 4u^2\varepsilon \quad (54)$$

will guarantee real, distinct roots. As in the continuous-time case, simplifying approximations can be made. The most conservative bound, analogous to (27), is

$$R_L > 2\sqrt{\frac{L}{C}}. \quad (55)$$

The experimental boost converter of Section III-D can be analyzed in discrete time as an example. A summary of results is shown in Table II, where distinct, real eigenvalues indicate timescale separation. In general, the bound of (55) is too conservative—the latter two configurations satisfy the necessary condition (54) and therefore exhibit timescale separation, but do not satisfy (55). Designers should focus on the more complicated requirement (54) to minimize losses.

Faster switching generally leads to less separation since p^2 is a significant factor in the discriminant. From another perspective, a lower sampling rate leads to more separation. Although the sampled-data model derived in (51) presumes a sampling rate equal to the switching frequency, this need not be the case. If the eigenvalues are real and distinct, even a small difference will become substantial over many switching cycles. For example, for the case where additional resistance is added in series with the inductor, the eigenvalues of Φ for a 25-kHz switching frequency are {0.9678, 0.8684}. If both the switching frequency

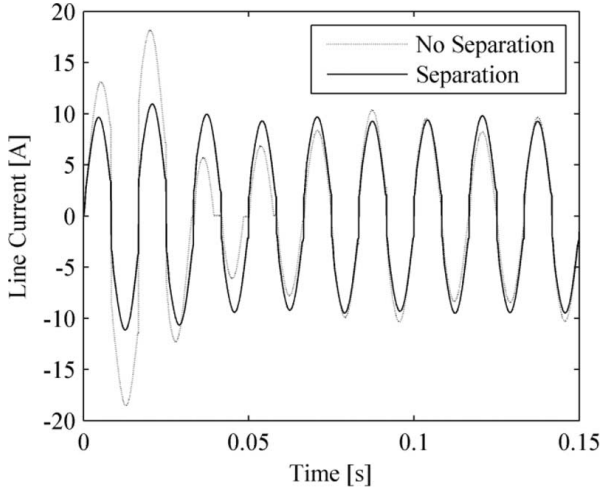


Fig. 11. Simulated PFC boost converter. Line current shown for two values of R_L : $80 \text{ m}\Omega$ (no separation) and 1.28Ω (separation).

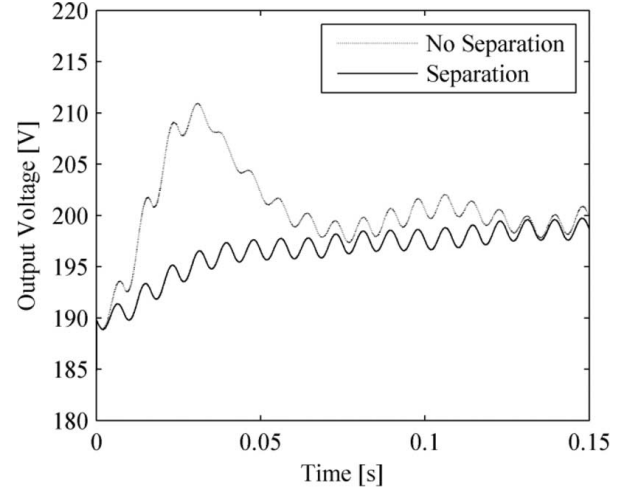


Fig. 12. Simulated PFC boost converter. Output (capacitor) voltage shown for the same two cases as in Fig. 11.

and sampling rate are increased to 250 kHz, the eigenvalues are $\{0.9969, 0.9861\}$ —a small difference. If the sampling rate is left at 25 kHz, but the switching frequency is set to 250 kHz, the eigenvalues are $\{0.9697, 0.8696\}$ —nearly the same as with 25-kHz switching. Over the range where the converter remains in continuous conduction mode, increased switching frequency narrows the apparent difference between timescales, while separation is retained if sampling rate remains constant regardless of the switching frequency.

VI. APPLICATION TO A PFC CONVERTER

PFC boost converters rely on timescale separation for effective operation. A simulation has been constructed to demonstrate the effect of R_L on dynamic performance, since an experimental PFC converter that does not exhibit timescale separation will not function well enough for extended testing. The simulated converter has 5 mH of line inductance, 5 mF of output capacitance, and switches at 75 kHz. The two cases have different values of parasitic resistance R_L : $80 \text{ m}\Omega$ and 1.28Ω . The control law combines feedback and feedforward

$$u = \frac{V_{\text{in}}}{V_0 + 10 \int (V_0 - v_C) dt}. \quad (56)$$

Although the line current is not sensed or explicitly controlled, the control of (56) produces current that is nearly sinusoidal. There is a small dc offset in the inductor current, which shows up as zero-crossing distortion in the line current. A longer simulation would show that the dc component decays to zero and has little effect on long-term performance. Figs. 11 and 12 show the line current and bus voltage start-up transients, respectively, for two converters with different R_L . With R_L being too small, there is no separation, and a second-order oscillation with overshoot is observed. With additional damping, the current magnitude and average voltage show first-order behavior. The estimated efficiency with separation exceeds 93%. A larger

output capacitor would enable separation with less damping and higher efficiency.

VII. CONCLUSION AND EXTENSIONS

Timescale separation is important in many applications, from PFC to low-voltage dc–dc converters. Separation criteria were derived for boost, buck, and buck–boost converters in both continuous-time and discrete-time formulations. The relationship among inductance, capacitance, and the inductor’s parasitic resistance dominated the results. An experimental boost converter, with both resistive and constant-power loads, demonstrated the effects of various design choices. A simulated PFC converter showed that extremely simple controllers can produce good line current waveforms if there is timescale separation.

Designers may use these results in several ways. If a particular converter is already designed, then the control designer may check the criteria before choosing a particular control methodology. Alternatively, if a particular control scheme is desired, the power designer can make component choices that ensure separation. The separation criteria can also be used as constraints to improve a converter optimization problem.

Future work will explore similar concepts for other converter topologies and closed-loop systems. In more complicated topologies, such as boost–buck or single-ended primary inductor converter (SEPIC), the presence of extra states complicates the analysis. Often, there are four or more states. Depending on component selection, there may be two, three, or four timescales. In a closed-loop system, the input u is no longer exogenous, but instead is a function of the states x and z , and the disturbance input w . The feedback system may itself contain extra states, and may either enhance or detract from timescale separation. As shown in the example PFC controller, though, a controller built entirely on the slow timescale will usually be effective if there is timescale separation.

APPENDIX
MATHEMATICA CODE FOR KBM ALGORITHM

A portion of this code is adapted from [19].

```
(* First define switched linear system *)
x={vCnorm,iLnorm};
T={0,duty*p,p};
nconfig=2;
amat={{1,h2},{-h2/ε,(δ0+h2*Rc/R)/ε}};
bmat={-w2,(Rc+R)*w1/(ε*R)-h2*w2*Rc/(ε*R)};

n=Length[x];
a={(amat/.{h1→1,h2→0}), (amat/.{h1→0,h2→1})};
b={(bmat/.{h1→1,h2→0}), (bmat/.{h1→0,h2→1})};

rhs=Table[a[[i]].x+b[[i]},{i,nconfig}];

(* Now perform KBM averaging per [19] *)
AVERAGE[f_]:=Cancel[(1/p)
Sum[Integrate[f[[id0]],{t,T[[id0]],T[[id0+1]]}],{id0,nconfig}]];

PDER[fv_,v_]:=Table[D[fv[[id1]],v[[jd1]],{id1,n},{jd1,n}];

KBMAgorithm[rhspsi_,Gold_,psiold_,Golder_,psiolder_]:=Block[{i,
G=AVERAGE[rhspsi];
psidi=Simplify[Table[Integrate[rhspsi[[i]]-G-
PDER[psiolder[[i]],x].Gold-
PDER[psiold[[i]],x].Golder,t],{i,nconfig}]];
psibc={psidi[[1]]};
Do[AppendTo[psibc,Cancel[psidi[[i]]+(psibc[[i-1]]/.t→T[[i]])-
(psidi[[i]]/.t→T[[i]])]],{i,2,nconfig}];
psiavg=AVERAGE[psibc];
psi=Table[psibc[[i]]-psiavg,{i,nconfig}]];

zerovec=Table[0,{i,n}];
zeromat=Table[zerovec,{i,nconfig}];

KBMAgorithm[rhs,zerovec,zeromat,zerovec,zeromat]
G1=Simplify[G]
Ψ1=Simplify[psi];
Ψavg1 = Simplify[psiavg];
Ψdi1 = Simplify[psidi];

apsi=Table[a[[j]].Ψ1[[j]},{j,nconfig}];
KBMAgorithm[apsi,G1,zeromat,zerovec,Ψ1]
G2=Simplify[G] (* Always zero *)
Ψ2=Simplify[psi];

apsi=Table[a[[j]].Ψ2[[j]},{j,nconfig}];
KBMAgorithm[apsi,g2,Ψ2,g1,Ψ1]
G3=Simplify[G]

(* Form normalized system from average plus one switching term *)
f = G1[[1]]+G3[[1]]
g = ε*(G1[[2]]+G3[[2]])
intermediate = Solve[g==0,iLnorm]
(* Now find manifold for z and off-manifold dynamics *)
φ0 = (iLnorm /. intermediate)[[1]]
φ1 = (1/D[g,iLnorm])*(D[φ0,vCnorm])*(f /. iLnorm → φ0)
ηrhs = (g /. iLnorm → (φ0 + ε*φ1 + η))-ε*(D[φ0,vCnorm])*(f /. iLnorm →
(φ0+η));
simpleηrhs = Simplify[ηrhs]

(* For stability, need η coefficient to be negative *)
ηcoeff = D[simpleηrhs,η]

(* Discard switching term, see what effect it has *)
infinitef = Simplify[simpleηrhs /. p → 0]
Solve[D[infinitef,η]==0, ε]
infinitefφ0 = φ0 /. p → 0
infinitefφ1 = φ1 /. p → 0
Simplify[infinitefφ1]
infinitefηcoeff = ηcoeff /. p → 0
Simplify[infinitefηcoeff]
```

REFERENCES

- [1] P. Athalye, D. Maksimović, and R. Erickson, "Variable-frequency predictive digital current mode control," *IEEE Power Electron Lett.*, vol. 2, no. 4, pp. 113–116, Dec. 2004.
- [2] S. Bibian and H. Jin, "High performance predictive dead-beat digital controller for DC power supplies," *IEEE Trans. Power Electron.*, vol. 17, no. 3, pp. 420–427, May 2002.
- [3] F. Blaabjerg, P. C. Kjaer, P. O. Rasmussen, and C. Cossar, "Improved digital current control methods in switched reluctance motor drives," *IEEE Trans. Power Electron.*, vol. 14, no. 3, pp. 563–572, May 1999.
- [4] S. Chattopadhyay, V. Ramanarayanan, and V. Jayashankar, "A predictive switching modulator for current mode control of high power factor boost rectifier," *IEEE Trans. Power Electron.*, vol. 18, no. 1, pp. 114–123, Jan. 2003.
- [5] J. Chen, A. Prodić, R. Erickson, and D. Maksimović, "Predictive digital current programmed control," *IEEE Trans. Power Electron.*, vol. 18, no. 1, pp. 411–419, Jan. 2003.
- [6] D. G. Holmes and D. A. Martin, "Implementation of a direct digital predictive current controller for single and three phase voltage source inverters," in *Proc. IEEE Ind. Appl. Conf.*, 1996, pp. 906–913.
- [7] Y.-S. Jung, "Small-signal model-based design of digital current-mode control," *Proc. Inst. Electr. Eng. Electr. Power Appl.*, vol. 152, pp. 871–877, Jul. 2005.
- [8] P. Mattavelli, "Digital control of dc–dc boost converters with inductor current estimation," in *Proc. Appl. Power Electron. Conf.*, 2004, pp. 74–80.
- [9] C.-T. Pan, Y.-S. Huang, and C.-Y. Li, "An error bounded current controller with constant sampling frequency," *IEEE Trans. Power Electron.*, vol. 19, no. 3, pp. 739–747, May 2004.
- [10] H. Peng and D. Maksimović, "Digital current-mode controller for dc–dc converters," in *Proc. Appl. Power Electron. Conf.*, 2005, pp. 899–905.
- [11] O. García, J. A. Cobos, R. Prieto, P. Alou, and J. Uceda, "Single phase power factor correction: A survey," *IEEE Trans. Power Electron.*, vol. 18, no. 3, pp. 749–755, May 2003.
- [12] J. W. Kimball, "Digital control techniques for switching power converters," Ph.D. dissertation, Univ. Illinois, Urbana, 2007.
- [13] J. W. Kimball and P. T. Krein, "Singular perturbation theory for dc–dc converters and application to PFC converters," in *Proc. IEEE Power Electron. Spec. Conf.*, 2007, pp. 882–887.
- [14] P. V. Kokotović, H. K. Khalil, and J. O'Reilly, *Singular Perturbation Methods in Control: Analysis and Design*. London, U.K.: Academic, 1986.
- [15] P. T. Krein, J. Bentsman, R. M. Bass, and B. L. Lesieutre, "On the use of averaging for the analysis of power electronic systems," *IEEE Trans. Power Electron.*, vol. 5, no. 2, pp. 182–190, Apr. 1990.
- [16] R. D. Middlebrook, "Small-signal modeling of pulse-width modulated switched-mode power converters," *Proc. IEEE*, vol. 76, no. 4, pp. 343–354, Apr. 1988.
- [17] R. D. Middlebrook and S. Čuk, "A general unified approach to modeling switching converter power stages," in *Proc. IEEE Power Electron. Spec. Conf.*, 1976, pp. 18–34.
- [18] R. D. Middlebrook and S. Čuk, "A general unified approach to modeling switching dc-to-dc converters in discontinuous conduction mode," in *Proc. IEEE Power Electron. Spec. Conf.*, 1977, pp. 36–57.
- [19] P. T. Krein and R. M. Bass, "A new approach to fast simulation of periodically switching power converters," in *Proc. Ind. Appl. Soc. Annu. Meeting*, 1990, pp. 1185–1189.
- [20] B. Lehman and R. M. Bass, "Switching frequency dependent averaged models for PWM dc–dc converters," *IEEE Trans. Power Electron.*, vol. 11, no. 1, pp. 89–98, Jan. 1996.
- [21] S. R. Sanders, J. M. Noworolski, X. Z. Liu, and G. C. Verghese, "Generalized averaging method for power conversion circuits," *IEEE Trans. Power Electron.*, vol. 6, no. 2, pp. 251–259, Apr. 1991.
- [22] G. C. Verghese, M. E. Elbuluk, and J. G. Kassakian, "A general approach to sampled-data modeling for power electronic circuits," *IEEE Trans. Power Electron.*, vol. PEL-1, no. 2, pp. 76–89, Apr. 1986.
- [23] A. R. Brown and R. D. Middlebrook, "Sampled-data modeling of switching regulators," in *Proc. IEEE Power Electron. Spec. Conf.*, 1981, pp. 349–369.
- [24] R. G. Phillips, "Two-timescale discrete systems," M.S. thesis, Univ. Illinois, Urbana-Champaign, 1979.
- [25] P. V. Kokotović, "A Riccati equation for block-diagonalization of ill-conditioned systems," *IEEE Trans. Autom. Control*, vol. 20, no. 6, pp. 812–814, Dec. 1975.
- [26] E. C. Bekir, "Singular perturbation methods for discrete time systems," in *Proc. IEEE Conf. Decis. Control*, 1985, vol. 24, pp. 86–94.
- [27] F. Hoppensteadt and W. Miranker, "Multitime methods for systems of difference equations," *Stud. Appl. Math.*, vol. 56, pp. 273–289, Jun. 1977.
- [28] R. G. Phillips, "Reduced order modelling and control of two-timescale discrete systems," *Int. J. Control*, vol. 31, pp. 765–780, Apr. 1980.



Jonathan W. Kimball (M'96–SM'05) received the B.S. degree in electrical and computer engineering from Carnegie Mellon University, Pittsburgh, PA, in 1994, and the M.S. degree in electrical engineering and the Ph.D. degree in electrical and computer engineering from the University of Illinois at Urbana-Champaign, Urbana-Champaign, in 1996 and 2007.

From 1996 to 1998, he was with Motorola, Phoenix, AZ, where he was engaged in designing insulated gate bipolar transistor (IGBT) modules for industrial applications. He then joined Baldor Electric, Fort Smith, AR, where he designed industrial adjustable-speed drives ranging 1–150 hp. In 2003, he joined the University of Illinois as a Research Engineer, where he later became a Senior Research Engineer. In 2003, he co-founded SmartSpark Energy Systems, Inc., Champaign, IL, where he was Vice President of Engineering. In 2008, he joined Missouri University of Science and Technology (Missouri S&T), Rolla, where he is currently an Assistant Professor.

Dr. Kimball is a member of Eta Kappa Nu, Tau Beta Pi, and Phi Kappa Phi. He is a licensed Professional Engineer in the State of Illinois.



Philip T. Krein (S'76–M'82–SM'93–F'00) received the B.S. degree in electrical engineering and the A.B. degree in economics and business from Lafayette College, Easton, PA, and the M.S. and Ph.D. degrees in electrical engineering from the University of Illinois, Urbana.

He was an Engineer with Tektronix, Beaverton, OR. He then returned to the University of Illinois, where he is currently the Grainger Endowed Director's Chair in Electric Machinery and Electromechanics. His current research interests include all aspects of power electronics, machines, and drives, with emphasis on nonlinear control approaches. He authored an undergraduate textbook *Elements of Power Electronics* (Oxford University Press, 1998). In 2001, he helped initiate the International Future Energy Challenge, a student competition involving fuel-cell power conversion and energy efficiency. He holds 12 U.S. and four European patents. During 1997–1998, he was a Senior Fulbright Scholar at the University of Surrey, U.K.

Dr. Krein is a Registered Professional Engineer in Illinois and Oregon. He was recognized as a University Scholar in 1999, the highest research award at the University of Illinois. In 2003, he received the IEEE William E. Newell Award in Power Electronics. During 1999–2000, he was the President of the IEEE Power Electronics Society. From 2005 to 2007, he was a Distinguished Lecturer of the IEEE Power Electronics Society.